

Dynamics-based machine learning of transitions in Couette flow

Bálint Kaszás , Mattia Cenedese , and George Haller *

Institute for Mechanical Systems, ETH Zürich, Leonhardstrasse 21, 8092 Zürich, Switzerland



(Received 24 March 2022; accepted 4 August 2022; published 25 August 2022)

We derive low-dimensional, data-driven models for transitions among exact coherent states in one of the most studied canonical shear flows, the plane Couette flow. These one- or two-dimensional nonlinear models represent the leading-order reduced dynamics on attracting spectral submanifolds (SSMs), which we construct using the recently developed *SSMLearn* algorithm from a small number of simulated transitions. We find that the energy input and dissipation rates provide efficient parametrizations for the most important SSMs. By restricting the dynamics to these SSMs, we obtain reduced-order models that also reliably predict nearby, off-SSM transitions that were not used in their training.

DOI: [10.1103/PhysRevFluids.7.L082402](https://doi.org/10.1103/PhysRevFluids.7.L082402)

I. INTRODUCTION

A detailed analysis of complex nonlinear dynamical systems, such as those arising in fluid mechanics, generally requires reduced-order models. The two main reduction techniques available for this purpose are the proper orthogonal decomposition (POD) [1] and the dynamic mode decomposition (DMD) [2]. The POD approach is equation driven, projecting the governing equations onto an empirically selected set of most energetic modes. In contrast, the DMD approach is data driven, fitting a linear dynamical system to the dynamics of a set of observables. Neither of these approaches is, therefore, designed for a purely data-driven modeling of essentially nonlinear (or nonlinearizable) behavior [3].

A hallmark of nonlinearizability on a domain of the phase space of a dynamical system is the coexistence of isolated stationary states (called invariant solutions in the fluid dynamics literature [4]) and transitions among them, which are as ubiquitous in laminar Couette flows as in turbulent pipe flows. Several emerging machine learning techniques could formally be applied to pattern-match transitions in such flows. These techniques, however, are not yet mature enough to produce physically interpretable models of reasonable complexity that can reliably predict the dynamics for initial conditions not used in their training [5].

A recent approach reduces nonlinearizable dynamics to spectral submanifolds (SSMs) [6,7], which are the smoothest nonlinear continuations of invariant (spectral) subspaces of the linearized system near a stationary state, such as a fixed point, a periodic orbit, or a quasiperiodic torus [6]. Building on more abstract prior work by Refs. [8,9], SSM theory establishes the existence and uniqueness of spectral submanifolds if the eigenvalues corresponding to the spectral subspace are not in resonance with the rest of the spectrum. See Supplemental Material [10] for more details. In the vicinity of the smoothest (primary) SSM, other, less smooth (secondary) SSMs also exist. Coexisting stationary states might also be contained in such secondary SSMs [11] in a vicinity of the smoothest SSM, as indeed turns out to be the case here. Restricting the governing equations to such low-dimensional attracting SSMs, therefore, provides a fast and mathematically exact model reduction procedure, as has been demonstrated for finite-element models of beams, shells, and

*georgehaller@ethz.ch

wings, with degrees of freedom ranging up to hundreds of thousands [12]. Due to the invariance of the SSM used in the model order reduction, the accuracy of the computed models depends only on the accuracy of the numerical approximation for the SSMs. This can be gradually enhanced by increasing the polynomial order of expansion for the SSM without increasing the dimension of the reduced model. SSM-based reduction has yielded highly accurate and predictive reduced models of very high-dimensional finite-element equations [12,13].

Very recently, SSM-based model reduction has been extended to a fully data-driven setting [11]. Implemented in the open-source *SSMLearn* package, the algorithm identifies the most influential nonresonant spectral subspaces near a stationary state from a linear modal analysis of a few training trajectories. It then proceeds to construct the corresponding nonresonant SSMs and the extended normal form of their reduced dynamics from the training data. The resulting SSM-based models have proven to be accurate in predicting behavior in several problems from solid and fluid mechanics, even under the addition of external forcing absent in their training data [11,14,15].

It has been unclear, however, whether data-driven SSM reduction can also describe transitions among coexisting stationary states accurately. Such phenomena are omnipresent in a number of outstanding problems of applied science, such as transitions to turbulence [4] and tipping points [16] in climate. To examine the applicability of the SSM-based approach to these grand challenges, it is feasible start with similar but simpler canonical problems that are nevertheless of significant interest in their own right. In this Letter, we will carry out such an exploratory study for one of the most studied classic shear flows, the plane Couette flow.

The anchor points of SSM theory, stationary states, have been broadly studied in the Couette flow literature as exact coherent states (ECSs) [17,18]. These can be equilibrium points, traveling waves, periodic orbits, quasiperiodic trajectories, or even chaotic attractors. Transitions between ECSs are generally understood to happen along their stable and unstable manifolds [18–23]. This is even supported by experimental observations [24]. Yet, with the exception of the two-dimensional unstable manifold of the base state in the flow past a cylinder [25], the role of invariant manifolds emanating from ECSs has not yet been systematically explored in model reduction.

An added motivation is recent work on the applicability of linear data-driven modeling tools to transitions between ECSs in plane Couette flow [3]. The conclusion of that study is that while DMD can feature-match individual transition trajectories over certain time intervals, no underlying convergent Koopman mode decomposition [26] justifying such a formal DMD analysis exists beyond subsets of the domains of attraction or repulsion of the ECSs. In more practical terms, while linear model reduction methods fitted to nonlinearizable data sets always return a closest-fitting linear model, the predictive power of such a model is limited to an *a priori* unknown subset of the phase space that contains a single stable or unstable ECS. Capturing multiple ECSs and the transitions among them in a single reduced-order model for Couette flows has been, therefore, an outstanding challenge which we wish to address here using data-driven, SSM-based nonlinear model reduction. Specifically, we seek to compute the most influential SSMs and their reduced dynamics in the phase space via the dynamics-based machine learning approach of Ref. [11]. We rely solely on simulation data, which renders our approach nonintrusive. We parametrize the SSMs with physically interpretable observables used in earlier studies of this flow to obtain very low- (one- or two-) dimensional dynamical systems for these observables along the SSMs. We also assess the predictive power of these reduced models for nearby trajectories starting off the SSMs. In this Letter, we seek the parametrization of SSMs and their reduced dynamics using classical machine learning techniques, such as polynomial regression. Based on the mathematical existence results on SSMs, one can also seek SSM-based models with more advanced tools from machine learning [27]. We refer to the Supplemental Material [10] and the *Matlab* live scripts under Ref. [28] for more information on our data sets and computations.

II. SETUP

We consider the plane Couette flow configuration [29]: an incompressible fluid flow between two infinite plates moving in opposite directions. The velocity field $\mathbf{u} = [u, v, w](x, y, z, t)$ evolves

according to the Navier-Stokes equations along with the pressure p ,

$$\frac{\partial \mathbf{u}}{\partial t} + \mathbf{u} \cdot \nabla \mathbf{u} = -\nabla p + \frac{1}{\text{Re}} \Delta \mathbf{u}, \quad \nabla \cdot \mathbf{u} = 0, \quad (1)$$

in the physical domain $\Omega = [0, L_x] \times [-h, h] \times [0, L_z]$, where the Reynolds number is defined as $\text{Re} = Uh/\nu$, with ν denoting the kinematic viscosity, h is half the distance between the plates, and U is their velocity. Our equations are nondimensionalized by the plate velocity U and the half width of the channel h . As in previous studies [3,30], we impose periodic boundary conditions in the x (spanwise) and z (streamwise) directions and in the wall normal direction we require $u(x, y = \pm 1, z, t) = \pm 1$. With the choice $L_x = 5\pi/2$ and $L_z = 4\pi/3$, our computational cell is comparable to those used in Refs. [3,31].

We solve Eq. (1) using the open source *Channelflow* library [32], with a spectral discretization of $32 \times 35 \times 32$ modes, resulting in a phase space of dimension $O(10^5)$. This is a very high but still finite-dimensional phase space to which the mathematical results behind *SSMLearn* are directly applicable. We rely on *Channelflow* only for generating trajectories, which we use for training and testing our SSM-based, data-driven models via the open source toolbox *SSMLearn* [11].

Here, we focus on the low Reynolds number regime in which the plane Couette flow is bistable [30]. In this geometry, at around $\text{Re} = 134.5$, the lower and upper branch of fixed points first observed by Nagata [33] appear in a saddle-node bifurcation. We restrict all calculations to the invariant subspace of the group generated by the shift-reflect and shift-rotate symmetries [18], the isotropy subgroup of the Nagata equilibria. This restriction ensures that the stationary states we study become hyperbolic, i.e., their spectrum does not contain the zero eigenvalues arising from the transnational invariance of the governing equations. Hyperbolicity of the stationary states is required for all SSM results to apply and also insures the robustness (structural stability) of our results. All orbits connecting these hyperbolic stationary states also remain in this invariant subspace.

Together with the constant-shear base state, $\mathbf{u}_{\text{base}} = [u = y, v = 0, w = 0]$, the Nagata equilibria represent the simplest examples of ECSs, with transitions among them along SSMs. Specifically, trajectories close to the unstable fixed point evolve along the unstable manifold that connects into slow SSMs of the two attracting states. At higher Re , nontrivial ECSs (e.g., periodic or quasiperiodic orbits) start appearing via bifurcations [34].

Our aim here is to develop reduced models on SSMs that predict transitions between three coexisting ECSs based on a small number of simulated transitions. To parametrize the SSMs, we choose physically relevant quantities from previous studies of the same flow [18,34], such as the rate of energy input (I) supplied by the walls and the rate of energy dissipation (D) due to friction, often used to get a projected representation of the Navier-Stokes equations [18,34,35], motivated by an energy balance of the flow [36]. Considering the time dependence of the total energy defined as

$$E = \frac{\|\mathbf{u}(t)\|_{L^2}^2}{2} = \frac{1}{2L_x L_z} \int_0^{L_x} \int_{-1}^1 \int_0^{L_z} \frac{|\mathbf{u}(x, y, z, t)|^2}{2} dz dy dx, \quad (2)$$

one can derive the differential equation governing $E(t)$ by taking the inner product of the Navier-Stokes equations with the velocity field \mathbf{u} and integrating over the flow domain Ω . Due to incompressibility and periodicity, one obtains [37]

$$\dot{E} = (I - D)/\text{Re}, \quad (3)$$

where the rate of energy input I and the dissipation D are defined as

$$I = \frac{1}{2L_x L_z} \int_0^{L_x} \int_0^{L_z} \left[\left(\frac{\partial u}{\partial y} u \right)_{y=1} + \left(\frac{\partial u}{\partial y} u \right)_{y=-1} \right] dz dx - 1, \quad (4)$$

$$D = \frac{1}{2L_x L_z} \int_0^{L_x} \int_{-1}^1 \int_0^{L_z} |\nabla \times \mathbf{u}|^2 dz dy dx - 1, \quad (5)$$

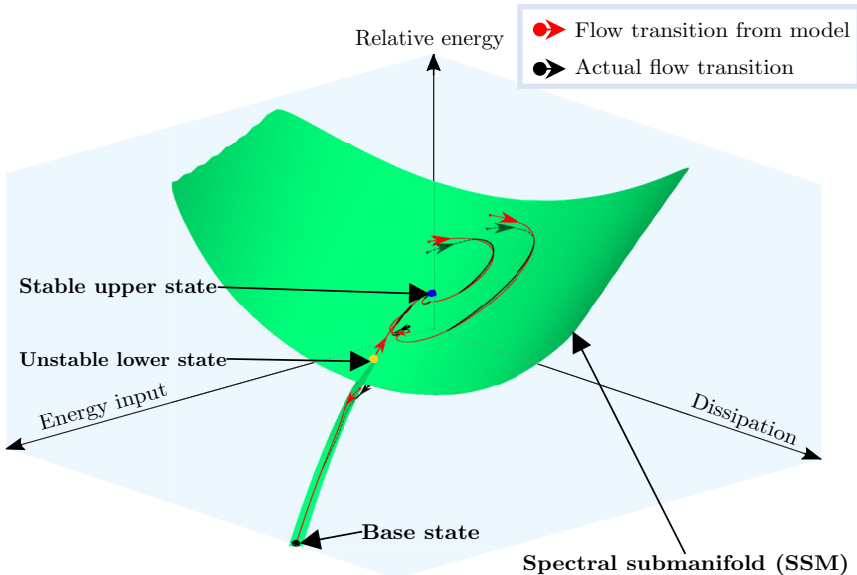


FIG. 1. Phase space geometry of plane Couette flow, projected onto the space of three observables: the relative energy ΔE , the energy input rate I , and the energy dissipation rate D . The three coexisting fixed points are the constant-shear base state (black dot), the unstable Nagata lower branch (yellow dot), and the stable Nagata upper branch (blue dot) fixed points. A two-dimensional SSM approximated by Eq. (7), containing all three fixed points, is shown in green. Due to the large distance between the base state and the lower Nagata equilibrium, we indicate the base state at a higher ΔE value along the manifold. Also shown are model-predicted and actual transitions between ECSs.

in order to measure these quantities relative to the constant shear base state. Another energy variable we use is $\Delta E = \|\mathbf{u}(t) - \mathbf{u}_{\text{base}}\|_{L^2}^2/2$. Our definitions ensure that $\Delta E = D = I = 0$ at the base state.

Parametrizations depending on I and D suffer from a singularity at the base state $I = D = 0$ due to their quadratic-type dependence on the velocity [cf. Eqs. (4) and (5)]. To remedy this problem without losing physical motivation, we choose $J = \sqrt{|I|}$ and $K = \sqrt{|D|}$ as parametrization variables (see the Supplemental Material). *SSMLearn* then reveals a smooth dependence of the reduced dynamics on the SSM graphed over this set of variables. Figure 1 shows an SSM, parametrized by (J, K) , plotted in the three-dimensional space $(I, D, \Delta E)$ with its dynamics describing transitions between ECSs.

III. RESULTS

Within the Reynolds number interval $[134.5, 150]$, we focus our analysis either on the unstable manifold of the lower branch fixed point or the slowest stable SSM of the stable limit cycle bifurcating from the upper branch fixed point. The unstable manifold of the lower branch is known to be one dimensional for a wide range of Reynolds numbers [38], making that fixed point an edge state [39–41]. As a result, we also find a one-dimensional connection between the lower branch fixed point and the stable base state. As for the upper branch, we distinguish three Reynolds number regimes, denoted by (I), (II), and (III) in Fig. 2, with different SSM geometries.

In region (I), close to the saddle-node bifurcation, the one-dimensional unstable manifold of the lower branch arrives necessarily tangent to the slowest SSM of the upper branch. This unstable manifold forms a heteroclinic connection between the two fixed points [42]. In this region, the slow SSM of the upper branch contains two heteroclinic connections: one between the lower and upper branch fixed point and one between the lower branch fixed point and the base state, as shown in Fig. 2(c).

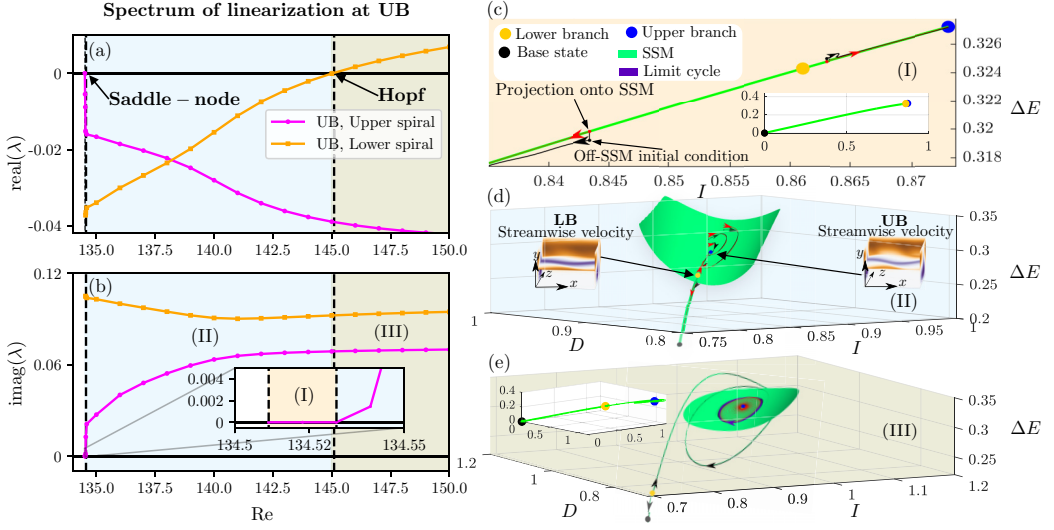


FIG. 2. Spectral submanifolds (SSMs) with different dimensions. (a) and (b) show the real and imaginary parts of the least stable eigenvalues λ of the upper branch (UB) fixed point. The upper spiral (magenta curve) has a larger real part after the saddle-node bifurcation than the lower spiral (orange curve). In the shaded region marked by (I), the SSM is one dimensional, while in regions (II) and (III), it is two dimensional. In region (III), it also contains a stable limit cycle. (c)–(e) show the SSMs and the coherent states contained in them in the corresponding regions. In the insets of (d) the streamwise velocity of the lower and upper branch fixed points is shown color coded. (d) and (e) are not to scale.

This alignment, however, breaks down at $\text{Re} = 134.53$ in region (II). The slowest SSM of the upper branch becomes two dimensional due to a collision of the least stable and second least stable eigenvalues, resulting in a pair of complex conjugate eigenvalues. After this secondary bifurcation, the upper branch becomes a stable spiral-type fixed point, preventing global one-dimensional SSM-based reductions. The heteroclinic connections, however, still exist in the two-dimensional slowest SSM of the upper branch fixed point, as shown in Fig. 2(d).

The upper branch undergoes yet another bifurcation at $\text{Re} = 145$, losing stability in a Hopf bifurcation leading to a stable limit cycle in region (III). After this point, the heteroclinic connection between the lower and upper branches disappears. Instead, an orbit connects the lower branch fixed point with the newly born limit cycle. As shown in Fig. 2(e), the two-dimensional unstable manifold of the upper branch fixed point forms the slowest stable SSM of the limit cycle. The unstable manifold of the lower branch fixed point shoots into a higher-dimensional SSM of the limit cycle.

To parametrize these SSMs, we use the square root of energy input J in the one-dimensional region (I) and the square roots of energy input and dissipation (J, K) in the two-dimensional regions (II) and (III), all centered at the base state. We seek parametrizations of the form

$$\mathbf{u}(x, y, z, t) = \mathbf{u}_{\text{base}} + \sum_{l=1}^M \mathbf{w}_l^{(1)}(x, y, z, \text{Re}) J^l(t) \quad (6)$$

or

$$\mathbf{u}(x, y, z, t) = \mathbf{u}_{\text{base}} + \sum_{\substack{l,m \\ l+m \leq M}} \mathbf{w}_{l,m}^{(2)}(x, y, z) J^l(t) K^m(t). \quad (7)$$

The coefficients $\mathbf{w}_l^{(1)}$ and $\mathbf{w}_{l,m}^{(2)}$ are identified from data via regression, as described in the Supplemental Material [10]. The maximal polynomial order is $M = 6, 2,$ and 5 for regions (I)–(III),

respectively. We allow for Re dependence in polynomial coefficients only for region (I) because this domain is small enough for a simple linear approximation of the Re dependence to be justified.

We initialize the training trajectories for the SSM-based models to lie approximately on the heteroclinic orbits between the ECSs. To this end, we start from initial conditions of the form $\mathbf{u}_{\text{LB}} \pm \varepsilon \mathbf{v}$, where $\varepsilon = O(10^{-5})$, and \mathbf{v} is the unstable eigenvector of the lower branch fixed point. We compute the ECSs, and their eigenvalues and eigenvectors with a Newton-Krylov solver [43]. Each of these initial conditions lies on the heteroclinic orbits between the lower and either the upper branches or the base state, respectively. In region (III), we use a training trajectory starting from the unstable subspace of the upper branch fixed point. This is to ensure that our training data accurately represent the behavior near the SSM.

Once we have identified the SSM geometry in the space of velocity measurements [44], we turn to modeling the reduced dynamics of parametrizing variables, considering first cases (I) and (II). Using the training trajectories, which are sampled at integer time instants, we fit polynomial mappings of the form

$$J_{n+1} = R(J_n, \text{Re}) \quad \text{or} \quad \begin{pmatrix} J_{n+1} \\ K_{n+1} \end{pmatrix} = \begin{pmatrix} R_1(J_n, K_n) \\ R_2(J_n, K_n) \end{pmatrix}, \quad (8)$$

where we have parametric dependence for Re in case (I) that is able to capture the saddle-node bifurcation of the lower and upper branch fixed points [45]. Further details on the identified reduced discrete dynamical systems are given in the Supplemental Material [10].

In region (III), we were not able to construct a two-dimensional SSM model of the upper transition dynamics: The one-dimensional unstable manifold of the lower branch fixed point spirals onto a limit cycle and hence is not a differentiable manifold. One could still construct higher-dimensional SSMs that contain this orbit. Analyzing the spectrum of the limit cycle (see the Supplemental Material [10] for the spectrum), we find that including the second slowest mode in the underlying spectral subspace would lead to a four-dimensional model. Instead, we construct a local nonlinear model on the two-dimensional SSM given by the unstable manifold of the upper branch fixed point. This manifold contains the upper branch fixed point, the limit cycle, and transitions between them. In this case, we use the data-driven extended normal form construction of *SSMLearn*, which yields the continuous-time reduced model

$$\dot{\rho} = 0.00171\rho - 0.01063\rho^3 - 0.01350\rho^5, \quad (9)$$

$$\dot{\theta} = 0.09290 - 0.01671\rho^2 + 0.01003\rho^4. \quad (10)$$

The polar normal form variables (ρ, θ) are connected to (J, K) via a nonlinear change of coordinates [46], which is identified from data as we discuss in the Supplemental Material [10]. The data-driven model in (9) and (10) takes the form of a Stuart-Landau equation [47,48].

To illustrate the accuracy and predictive power of these discrete and continuous reduced-order models, we consider trajectories initialized away from the SSMs in all three cases. We consider an ensemble of randomly chosen initial conditions whose L^2 distance from the unstable lower state is 10^{-2} . Based on the SSM-reduced models we have obtained, we predict the time evolution of their $[J(t), K(t)]$ coordinates from $[J(0), K(0)]$ using Eqs. (8)–(10) and then extend these predictions into the full phase space using the graph of the corresponding SSM in Eqs. (6) and (7), with a final evaluation of the model prediction error $\|\mathbf{u}(t) - \mathbf{u}(t)_{\text{true}}\|_{L^2}$.

In Figs. 3(a)–3(c), we plot the time evolution of $I = J^2$ for a few members of the test ensemble. We found that the predictions based on the reduction to the SSM are qualitatively accurate as long as the trajectory does not start too far away from the SSM, where fast transients have a major influence on the dynamics. In Figs. 3(d)–3(f), we show the relative reconstruction error for the test ensemble. The error is normalized by the maximum value of the L^2 norm of the true trajectory.

IV. CONCLUSIONS

These results illustrate the power of SSM-based, data-driven reduced-order models for nonlinearizable transition dynamics in a canonical nonlinear fluid flow that has defied prior attempts to

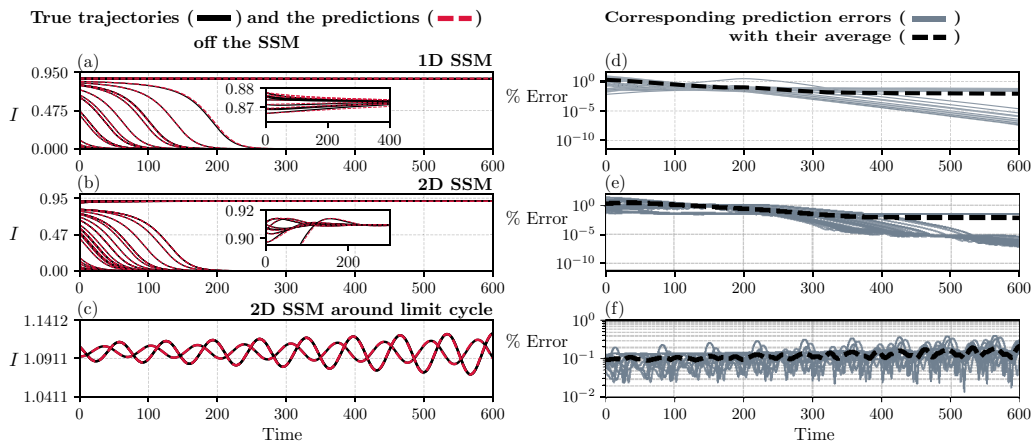


FIG. 3. Predictions from the reduced-order models. In (a)–(c) we show the predicted and true time evolutions of the variable I for trajectories starting close to the SSM. The Reynolds number is 134.52 in (a), 135 in (b), and 146 in (c). In (d)–(f) the prediction error $\|\mathbf{u}(t) - \mathbf{u}_{\text{true}}(t)\| / \max \|\mathbf{u}_{\text{true}}(t)\|$ is plotted in gray for the individual trajectories. The black dashed curve shows the average of the error over the ensemble of 50 trajectories in (d), (e) and 20 trajectories in (f).

derive such models. We have demonstrated that SSM-reduced nonlinear models can simultaneously capture coexisting ECSs and heteroclinic transitions among them, even in large distances from the stationary states serving as its anchor point. Importantly, our SSM-reduced models have also provided reliable predictions for transitions in open neighborhoods of the SSMs carrying them.

Consequently, more general tipping transitions [49,50], i.e., transitions between steady states induced by changing parameters or noise, are also expected to be captured by an appropriate SSM-based reduction. Although we only considered the SSMs at low Reynolds in this shear flow configuration, a similar analysis is, in principle, possible for higher Reynolds numbers. At even higher Reynolds numbers, the boundary of the domain of attraction of the base state (i.e., the stable manifold of the lower branch fixed point) becomes even more complicated, filled with unstable periodic orbits [35,51]. Reducing the dynamics to SSMs that are submanifolds of this edge offers hope for an SSM-based modeling of transition to turbulence.

Limitations of the present approach include the *a priori* unknown size of the domain of validity of the reduced-order model in the full phase space and the lack of an appropriate SSM-based reduced-order model for upper transitions in domain (III). Making progress on both of these challenges will require the construction of higher- (but still low-) dimensional invariant manifolds containing the upper transition orbits. Due to the simultaneous presence of both stable and unstable modes along such envisioned manifolds, the current SSM theory behind the *SSMLearn* algorithm needs technical extensions to accommodate both stable and unstable directions simultaneously.

The codes and a sample of the data used for the analysis are available under the link [28], in the form of a commented *Matlab* live script, as a part of the open-source toolbox *SSMLearn* [11]. The complete data set is available from the authors upon request.

ACKNOWLEDGMENTS

We are grateful to Jacob Page and Mingwu Li for useful discussions and their helpful comments. We acknowledge support from Priority Program SPP 1881 (Turbulent Superstructures) of the German National Science Foundation (DFG).

-
- [1] P. Holmes, J. L. Lumley, and G. Berkooz, *Turbulence, Coherent Structures, Dynamical Systems and Symmetry*, Cambridge Monographs on Mechanics (Cambridge University Press, Cambridge, UK, 1996).
- [2] P. J. Schmid, Dynamic mode decomposition and its variants, *Annu. Rev. Fluid Mech.* **54**, 225 (2022).
- [3] J. Page and R. R. Kerswell, Koopman mode expansions between simple invariant solutions, *J. Fluid Mech.* **879**, 1 (2019).
- [4] G. Kawahara, M. Uhlmann, and L. van Veen, The significance of simple invariant solutions in turbulent flows, *Annu. Rev. Fluid Mech.* **44**, 203 (2012).
- [5] S. Brunton, B. Noack, and P. Koumoutsakos, Machine learning for fluid mechanics, *Annu. Rev. Fluid Mech.* **52**, 477 (2020).
- [6] G. Haller and S. Ponsioen, Nonlinear normal modes and spectral submanifolds: Existence, uniqueness and use in model reduction, *Nonlinear Dyn.* **86**, 1493 (2016).
- [7] F. Kogelbauer and G. Haller, Rigorous model reduction for a damped-forced nonlinear beam model: An infinite-dimensional analysis, *J. Nonlinear Sci.* **28**, 1109 (2018).
- [8] X. Cabre, E. Fontich, and R. de la Llave, The parameterization method for invariant manifolds I: Manifolds associated to non-resonant subspaces, *Indiana Univ. Math. J.* **52**, 283 (2003).
- [9] A. Haro and R. de la Llave, A parameterization method for the computation of invariant tori and their whiskers in quasi-periodic maps: Rigorous results, *J. Differ. Equ.* **228**, 530 (2006).
- [10] See Supplemental Material at <http://link.aps.org/supplemental/10.1103/PhysRevFluids.7.L082402> for more information on the data sets and additional computations.
- [11] M. Cenedese, J. Axås, B. Bäuerlein, K. Avila, and G. Haller, Data-driven modeling and prediction of non-linearizable dynamics via spectral submanifolds, *Nat. Commun.* **13**, 872 (2022).
- [12] S. Jain and G. Haller, How to compute invariant manifolds and their reduced dynamics in high-dimensional finite element models, *Nonlinear Dyn.* **107**, 1417 (2022).
- [13] M. Li, S. Jain, and G. Haller, Nonlinear analysis of forced mechanical systems with internal resonance using spectral submanifolds—Part I: Periodic response and forced response curve, *Nonlinear Dyn.* (2022).
- [14] M. Cenedese, J. Axås, H. Yang, M. Eriten, and G. Haller, Data-driven nonlinear model reduction to spectral submanifolds in mechanical systems, *Philos. Trans. R. Soc. A* **380**, 20210194 (2022).
- [15] J. Axås, M. Cenedese, and G. Haller, Fast data-driven model reduction for nonlinear dynamical systems, [arXiv:2204.14169](https://arxiv.org/abs/2204.14169).
- [16] T. M. Lenton, H. Held, E. Kriegler, J. W. Hall, W. Lucht, S. Rahmstorf, and H. J. Schellnhuber, Tipping elements in the Earth’s climate system, *Proc. Natl. Acad. Sci. USA* **105**, 1786 (2008).
- [17] F. Waleffe, Exact coherent structures in channel flow, *J. Fluid Mech.* **435**, 93 (2001).
- [18] J. F. Gibson, J. Halcrow, and P. Cvitanović, Visualizing the geometry of state space in plane Couette flow, *J. Fluid Mech.* **611**, 107 (2008).
- [19] K. Fujimura, Centre manifold reduction and the Stuart-Landau equation for fluid motions, *Proc. R. Soc. London A* **453**, 181 (1997).
- [20] M. Carini, F. Auteri, and F. Giannetti, Centre-manifold reduction of bifurcating flows, *J. Fluid Mech.* **767**, 109 (2015).
- [21] N. B. Budanur and P. Cvitanović, Unstable manifolds of relative periodic orbits in the symmetry-reduced state space of the Kuramoto–Sivashinsky system, *J. Stat. Phys.* **167**, 636 (2017).
- [22] N. B. Budanur and B. Hof, Heteroclinic path to spatially localized chaos in pipe flow, *J. Fluid Mech.* **827**, R1 (2017).
- [23] M. Farano, S. Cherubini, J.-C. Robinet, P. De Palma, and T. M. Schneider, Computing heteroclinic orbits using adjoint-based methods, *J. Fluid Mech.* **858**, R3 (2019).
- [24] B. Suri, J. Tithof, R. O. Grigoriev, and M. F. Schatz, Forecasting Fluid Flows Using the Geometry of Turbulence, *Phys. Rev. Lett.* **118**, 114501 (2017).
- [25] J.-C. Loiseau, S. Brunton, and B. Noack, From the POD-Galerkin method to sparse manifold models, in *Model Order Reduction, Volume 3: Applications*, edited by P. Benner, S. Grivet-Talocia, A. Quarteroni, G. Rozza, W. Schilders, and L. Silveira (De Gruyter, Berlin, 2020), pp. 279–320.
- [26] C. W. Rowley, I. Mezić, S. Bagheri, P. Schlatter, and D. S. Henningson, Spectral analysis of nonlinear flows, *J. Fluid Mech.* **641**, 115 (2009).

- [27] T. Hastie, R. Tibshirani, and J. Friedman, *The Elements of Statistical Learning: Data Mining, Inference, and Prediction, Second Edition*, Springer Series in Statistics (Springer, New York, 2009).
- [28] B. Kaszás and M. Cenedese, Analysis of Couette flow regimes via SSMLearn. The data and the code is available under the repository, <https://github.com/haller-group/SSMLearn/tree/main/examples/couetteflow> (2022).
- [29] W. M. Orr, The stability or instability of the steady motions of a perfect liquid and of a viscous liquid. Part II: A viscous liquid, Proceedings of the Royal Irish Academy. Section A: Mathematical and Physical Sciences **27**, 69 (1907).
- [30] J. F. Gibson, J. Halcrow, and P. Cvitanović, Equilibrium and travelling-wave solutions of plane Couette flow, *J. Fluid Mech.* **638**, 243 (2009).
- [31] M. Nagata, Three-dimensional finite-amplitude solutions in plane Couette flow: Bifurcation from infinity, *J. Fluid Mech.* **217**, 519 (1990).
- [32] J. F. Gibson, F. Reetz, S. Azimi, A. Ferraro, T. Kreilos, H. Schrobdsdorff, M. Farano, A. F. Yesil, S. S. Schütz, M. Culp, and T. M. Schneider, Channelflow 2.0, <https://channelflow.ch>.
- [33] F. Waleffe, Homotopy of exact coherent structures in plane shear flows, *Phys. Fluids* **15**, 1517 (2003).
- [34] G. Kawahara and S. Kida, Periodic motion embedded in plane Couette turbulence: Regeneration cycle and burst, *J. Fluid Mech.* **449**, 291 (2001).
- [35] L. van Veen and G. Kawahara, Homoclinic Tangle on the Edge of Shear Turbulence, *Phys. Rev. Lett.* **107**, 114501 (2011).
- [36] C. R. Doering and P. Constantin, Energy Dissipation in Shear Driven Turbulence, *Phys. Rev. Lett.* **69**, 1648 (1992).
- [37] F. Waleffe, Overview of turbulent shear flows, in *Summer Program in Geophysical Fluid Dynamics* (Woods Hole Oceanographic Institution, Falmouth, MA, 2011).
- [38] J. Wang, J. Gibson, and F. Waleffe, Lower Branch Coherent States in Shear Flows: Transition and Control, *Phys. Rev. Lett.* **98**, 204501 (2007).
- [39] J. D. Skufca, J. A. Yorke, and B. Eckhardt, Edge of Chaos in a Parallel Shear Flow, *Phys. Rev. Lett.* **96**, 174101 (2006).
- [40] T. M. Schneider, J. F. Gibson, M. Lagha, F. De Lillo, and B. Eckhardt, Laminar-turbulent boundary in plane Couette flow, *Phys. Rev. E* **78**, 037301 (2008).
- [41] M. Avila, F. Mellibovsky, N. Roland, and B. Hof, Streamwise-Localized Solutions at the Onset of Turbulence in Pipe Flow, *Phys. Rev. Lett.* **110**, 224502 (2013).
- [42] J. Halcrow, J. F. Gibson, P. Cvitanović, and D. Viswanath, Heteroclinic connections in plane Couette flow, *J. Fluid Mech.* **621**, 365 (2009).
- [43] D. Viswanath, Recurrent motions within plane Couette turbulence, *J. Fluid Mech.* **580**, 339 (2007).
- [44] H. Whitney, The self-intersections of a smooth n -manifold in $2n$ -space, *Ann. Math.* **45**, 220 (1944).
- [45] H. Dankowicz and F. Schilder, *Recipes for Continuation* (SIAM, Philadelphia, 2013).
- [46] J. Guckenheimer and P. Holmes, *Nonlinear Oscillations, Dynamical Systems, and Bifurcations of Vector Fields*, Applied Mathematical Sciences Vol. 42 (Springer, Berlin, 2013).
- [47] J. T. Stuart, On the non-linear mechanics of hydrodynamic stability, *J. Fluid Mech.* **4**, 1 (1958).
- [48] L. D. Landau and E. M. Lifshitz, *Fluid Mechanics* (Pergamon Press, Oxford, UK, 1987).
- [49] P. Ashwin, S. Wieczorek, R. Vitolo, and P. Cox, Tipping points in open systems: Bifurcation, noise-induced and rate-dependent examples in the climate system, *Philos. Trans. R. Soc. A* **370**, 1166 (2012).
- [50] H. M. Alkhayuon and P. Ashwin, Rate-induced tipping from periodic attractors: Partial tipping and connecting orbits, *Chaos* **28**, 033608 (2018).
- [51] T. Kreilos and B. Eckhardt, Periodic orbits near onset of chaos in plane Couette flow, *Chaos* **22**, 047505 (2012).